SCIENCE CHINA
Information Sciences

• **Supplementary File** •

Controlled nano-cracking actuated by an in-plane voltage

Qiang LUO, Zhe GUO, Shuai ZHANG, Xiaofei YANG, Xuecheng ZOU, Jeongmin HONG & Long YOU*

School of Optical and Electronic Information, Huazhong University of Science and Technology, Wuhan 430074, China

Appendix A Randomly nanocracks induced in continuous MnPt film

To induce nanocracks in MnPt film, the MnPt films was first integrated on a double-polished PMN-PT substrate. Then, nanoscale silver paste was coated on the backside of PMN-PT substrate to be used as the bottom electrode. The device geometric structure and electrical measurement are schematically demonstrated in Figure A1(a). An out-of-plane triangular cyclic voltage V_C with an amplitude of 100 V and a period of 80 s was applied between the top MnPt film and the bottom Ag electrode. When V_C reverse swept from +100 V to -100 V, irregular cracks randomly distributed in the MnPt film can be observed under an optical microscope, as shown in Figure A1(b).

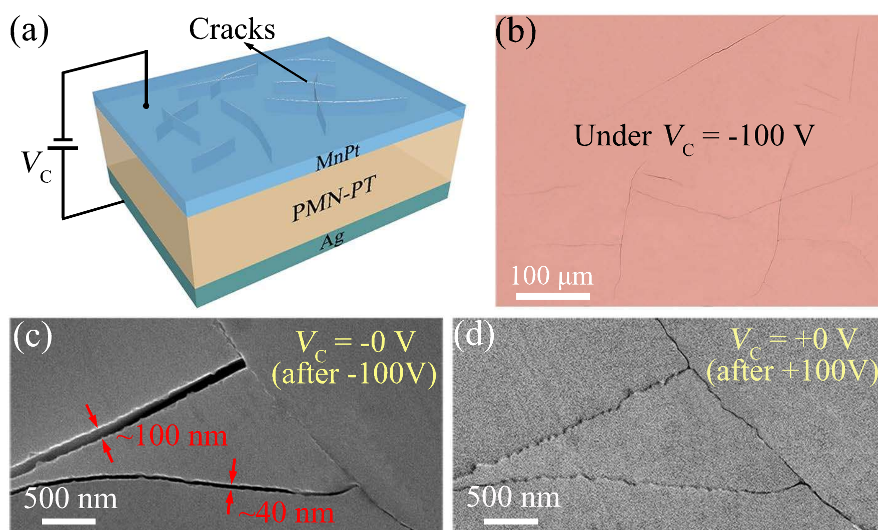

Figure A1 Randomly and irregularly distributed cracks in MnPt film under an out-of-plane voltage. (a) The device geometric structure and the schematic of the electrical measurement setup. (b) The local optical microscope image of the irregular cracks randomly distributed in the MnPt film. The SEM images of an (c) open-state and (d) closed-state of cracks in the MnPt film after sweeping the V_C from +100 to 0 V and -100 to 0 V, respectively.

To directly visualize the details of cracks, scanning electron microscopy (SEM) was utilized to image the cracks morphology as V_C was swept from -100 to 0 V and from +100 to 0 V, respectively. As shown in Figure A1(c), after sweeping V_C from -100 to 0 V, three interlaced cracks with a triangular distribution were in different states, two of which were open and the other was closed. After that, when V_C swept from +100 to 0 V, these two originally opened cracks changed to closed state, while the state of the other one remains unchanged (Figure A1d). Therefore, under the out-of-plane voltage, cracks are irregular and randomly distributed in the MnPt film. In addition, although non-volatile opening and closing of crack can be driven by such out-of-plane voltage, such switching is very complicated, which is not conducive to large-scale integrated applications.

Appendix B Experimental and analytical methods

(1) Materials preparation and fabrication of crack-based devices

The ferroelectric substrates used were (001)-oriented $[Pb(Mg_{1/3}Nb_{2/3})O_3]0.70$-$[PbTiO_3]0.30$ (PMN-PT) single crystal with the size of 5 x 5 x 0.5 mm^3 and double side polished. A MnPt intermetallic alloy thin film was integrated on the PMN-PT substrate.

* Corresponding author (email: lyou@hust.edu.cn)

Here, MnPt intermetallic alloy film was used mainly because of its two features: one is moderate mechanical property between ductile and brittle materials [1, 2], and the other one is excellent conductivity [3]. In actual experiment, a 40 nm MnPt thin film was deposited onto PMN-PT substrate from a $Mn_{50}Pt_{50}$ metallic target using a radio frequency (RF) magnetron sputtering system at room temperature. The Ar pressure was kept at 0.2 Pa and the RF source power was 20 W during the sputtering. After that, the MnPt film was patterned into designed structures via photolithography and argon ion milling. At the end, 20 nm Pt film was deposited on designed area by DC sputtering and lift-off process. The sputtering power and Ar pressure were kept at 20 W and 0.2 Pa, respectively.

(2) Cracks monitoring and morphology characterization

Electrical contacts onto electrodes area were made by electron probe with probe station. The crack generating and opening/closing state were monitored by an optical microscopy system with a digit charge coupled device (CCD) system. To induce the cracking, a triangular cyclic voltage was applied between the upper and lower electrodes via Keithley 2410 source meter. After the crack was induced, the dynamic opening and closing were visible under the CCD system. Then, the nonvolatile open- and closed-state of the crack was characterized by a Bruker AFM system.

(3) Electrical measurements

To control the crack states (open and closed), Keithley 2410 source meter was used to applied an in-plane cyclic control voltage between the upper and lower electrodes. During the voltage sweeping, the electrical resistance measurements were carried out by Keithley 2400 and 2450 source meters. A constant voltage across the crack and measured the channel current. Pulse measurements for repeatability testing were made by both Keithley 2410, 2400 and 2450 source meters.

(4) Electric field distribution simulations

The electric-field distribution of designed devices was analyzed using COMSOL Multiphysics software. The parameters and boundary condition of electric-field simulation are as follows:

(i) Parameters

The independent full matrix parameter of PMN-PT single crystal can be expressed as [4]:

$$\begin{pmatrix} c11 & c12 & c13 & c14 & c15 & c16 & d11 & d12 & d13 & d14 & d15 & d16 \\ c21 & c22 & c23 & c24 & c25 & c26 & d21 & d22 & d23 & d24 & d25 & d26 \\ c31 & c32 & c33 & c34 & c35 & c36 & d31 & d32 & d33 & d34 & d35 & d36 \\ c41 & c42 & c43 & c44 & c45 & c46 & \varepsilon 11 & \varepsilon 12 & \varepsilon 13 & & & \\ c51 & c52 & c53 & c54 & c55 & c56 & \varepsilon 21 & \varepsilon 22 & \varepsilon 23 & & \rho & \\ c61 & c62 & c63 & c64 & c65 & c66 & \varepsilon 31 & \varepsilon 32 & \varepsilon 33 & & & \end{pmatrix} \tag{B1}$$

In which, c_{ij} is the elastic stiffness constant under constant E, 10^{10} N/m^2;

d_{ij} is the dielectric constant under zero stress, 10^{-12} C/N;

ε is the dielectric constant under zero stress, ε_0;

ρ is the mass density, kg/m^3.

Specifically, the parameters of (001)-oriented PMN-30PT single crystal can be given in the following matrix [5]:

$$\begin{pmatrix} 16.04 & 14.96 & 7.51 & 0 & 0 & 0 & 0 & 0 & 0 & 0 & 592 & 0 \\ 14.96 & 16.04 & 7.51 & 0 & 0 & 0 & 0 & 0 & 0 & 592 & 0 & 0 \\ 7.51 & 7.51 & 12.0 & 0 & 0 & 0 & -1395 & -1395 & 2000 & 0 & 0 & 0 \\ 0 & 0 & 0 & 5.38 & 0 & 0 & 7093 & 0 & 0 & - & - & - \\ 0 & 0 & 0 & 0 & 5.38 & 0 & 0 & 7093 & 0 & - & 8093 & - \\ 0 & 0 & 0 & 0 & 0 & 2.87 & 0 & 0 & 6610 & - & - & - \end{pmatrix} \tag{B2}$$

(ii) Boundary condition

In the simulation, a PMN-PT single crystal poled along [001] direction was used as the ferroelectric substrate with the dimension of 5 mm x 5 mm x 0.5 mm. The thickness of MnPt layer was set to 40 nm. We simulated the electric-field distributions of the devices in two sizes. The side lengths of the triangular MnPt electrode areas were 100 μm and 1 μm, and the corresponding gap width between two separate MnPt electrodes were 30 μm and 300 nm, respectively.

In addition, the PMN-PT ferroelectric substrate was set to be insulated, and the MnPt electrode area was conductive. The in-plane voltage V_C was applied onto these two separate MnPt electrodes, in which, the upper electrode was used in grounding and $+V_C$ was applied onto the lower electrode. The V_C applied onto these three devices were 25 V and 1 V, respectively.

Appendix C Non-volatile switching of single-crack

For the non-volatile switching of single-crack, the optical image of the fabricated device was shown in Figure C1(a) and the enlarged image of the central region was shown in Figure C1(b). The dimension of central MnPt strip is 10 μm x 20 μm. The gap distance between the central MnPt strip and the upper/lower Pt electrodes (d_1 and d_2) are both 10 μm. In addition, the Pt electrodes at the left and right ends of the MnPt strip were used to prevent potential cracks generation in these areas.

The device structure is schematically demonstrated in Figure C2(a), in which the electrode C, D are used to induce and manipulate the crack. Moreover, the opening and closing state of crack can be confirmed by detecting the resistance between electrodes A and B. To induce crack, an in-plane triangular cyclic voltage (V_C) with an amplitude of 40 V and a period of 160 s (Figure C2b) was applied between C and D. After that, a switchable crack with microscale length was distinctly visible in the MnPt strip under the optical microscope (Figure 1a). To examine the effect of the crack switching (opening and closing) on the resistance of MnPt strip, the electrical resistance measurement was performed by a two-probes method, as shown in Figure C2(a). During the sweeping of V_C, the channel current I_{sd} was collected when a constant voltage of 1 mV was applied between A and B.

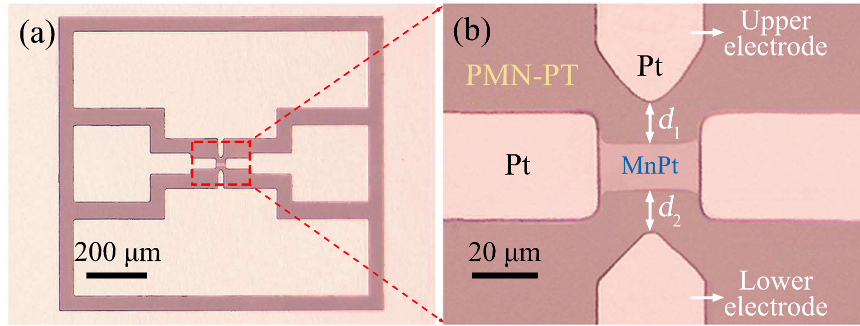

Figure C1 (a) The full-size optical images of the single-crack-based device; (b) The enlarged image of the central region.

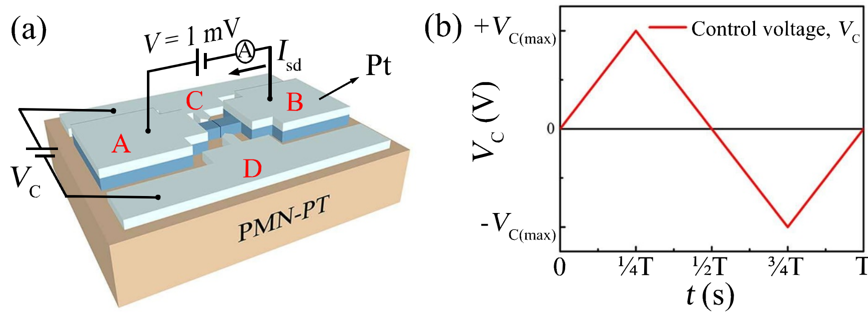

Figure C2 (a) Schematic of the electrical measurement geometry. (b) The electrical waveform for both inducing and manipulating crack.

Appendix D Complementary switching of two-crack

To prepare the complementary two-crack-based device, the MnPt thin film was directly etched into two separated triangular areas. The optical image of the fabricated device was shown in Figure D1(a). The side length of each triangular MnPt electrode is 100 μm, and the gap distance of these two electrodes is 30 μm. To induce the crack in each MnPt area, a cyclic V_C was applied between these two MnPt areas. The device structure and electric measurement geometry are represented in Figure D1(b). In each MnPt area, one crack will generate and then propagates through the MnPt area by applying an V_C between these two MnPt areas. Then, we also performed electrical resistance measurements for the complementary switching of these two cracks. A similar V_C with a smaller amplitude was used to control the complementary switching of these two cracks. A small constant voltage of 1 mV was applied across crack-1 and crack-2, respectively. Meanwhile, the channel currents I_1 and I_2 were measured.

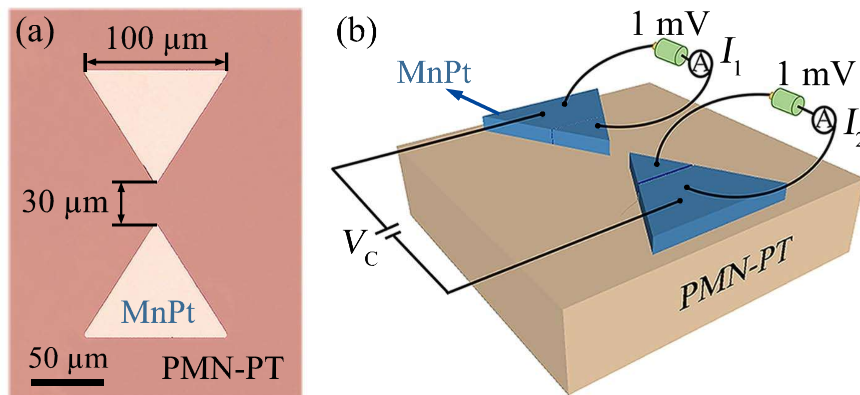

Figure D1 (a) The optical images of the complementary two-crack based device; (b) The schematic of the heterostructure and electrical measurement geometry.

The local morphology features of the crack-1 can be characterized by atomic force microscopy (AFM), as shown in Figure D2(a) and D2(b). As seen in Figure D2(a), the crack-1 is open with the gap width of 40 nm after scanning V_C from +50 to 0 V. In contrast, figure D2(b) shows a closed stated after V_C varied from -50 to 0 V. It should be note that these images were collected after removing V_C, indicating a non-volatile switching of crack.

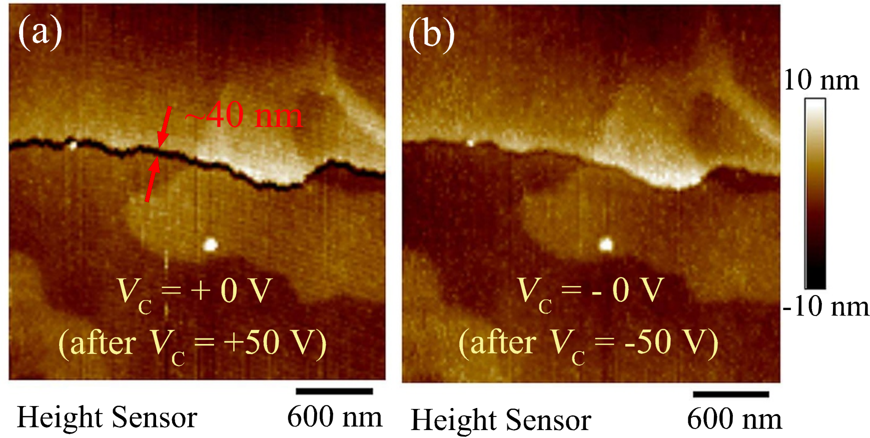

Figure D2 (a) and (b) AFM images of the crack-1 after scanning V_C from +50 to 0 V and from -50 to 0 V, respectively.

Appendix E Switching mechanism of cracks and device scaling

Figure E1(a) shows the schematic configuration of electric field decomposition. Obviously, the distributions of E_z in these two separated areas are in opposite directions, while E_y are always the same. The simulated E_x and E_y distributions are shown in Figure E1(b) and E1(c), respectively. Accordingly, the magnitude of E_x was close to zero values within these two triangular areas, and E_y was symmetric relative to x-axis, which is not in accordance with the complementary switching feature.

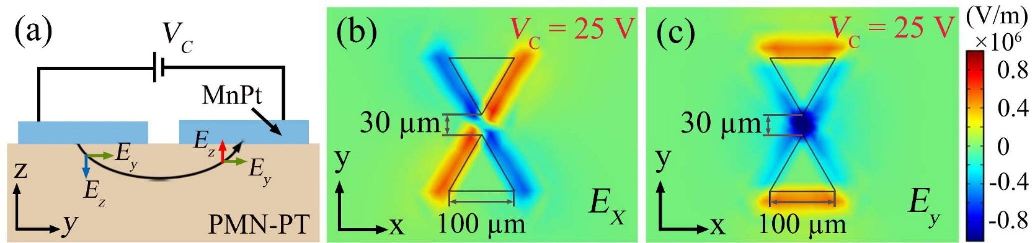

Figure E1 (a) Configuration of the electric field decomposition. (b)-(c) E_x and E_y distribution in the two-cracks-based device using COMSOL Multiphysics simulation.

Further, a series of devices with different dimensions and electrode shapes were fabricated to examine the reliability of crack formation and switching, as shown in Figure E2(a)-4(c). In our experiments, different switching behaviors of cracks can be easily achieved by designing simple device layouts. For instance, the switching of single-crack case (Figure E2a) and complementary switching of two-crack case (Figure E2b) can be effectively reproduced and manipulated by V_C. Interestingly, in our design, complementary switching of single-crack can be found, as shown in Figure E2(c). Similarly, under the V_C, one half of the crack will open and the other half will close, leading to a single-crack-based complementary switching. Thus, the crack formation and switching can be effectively controlled via such patterned structures, which would offer a scalable and flexible route to construct energy-efficient and high-density crack-based applications.

Appendix F Application for energy-efficient and high-density reconfigurable logic (RL)

The optical image of a two-crack based device with separated input and output signal paths for RL application is shown in Figure F1(a), and the enlarged detail view of the central region is shown in Figure F1(b). The gap width between the upper and lower Pt electrodes (d_1) is 10 μm and the dimensions of top end region of these two electrodes are both 6 μm x 40 μm. In addition, the dimensions of the MnPt strips on either side of the central Pt electrodes are both 6 μm x 30 μm, and the gap widths between the MnPt strip and the central Pt electrode (d_2 and d_3) are both 6 μm.

Such device mainly consists of two parts: (1) two cracks with complementary switching in Pt electrodes actuated by V_C, (2) the current readout path in MnPt intermetallic strips controlled by the states of extended cracks. During writing operation, the cracks states are determined by applying V_C onto these two Pt electrodes. While a non-destructive readout operation is performed by examining the currents across the cracks in MnPt strip using a constant voltage of 1 mV.

For the endurance measurement, it should be noted that the ON-state of the device will be unsustainable with an increase of the number of switching cycles, which is caused by the contact contamination of electrode material and the uneven contact surface. In the future, an ultra-high endurance of such crack-based device can be realized by using the robust contact material and the ferroelectric material with regular domain structure [6, 7].

References

1 Liu Z Q, Liu J H, Biegalski M D, et al. Electrically reversible cracks in an intermetallic film controlled by an electric field. Nat Commun, 2018, 9: 41

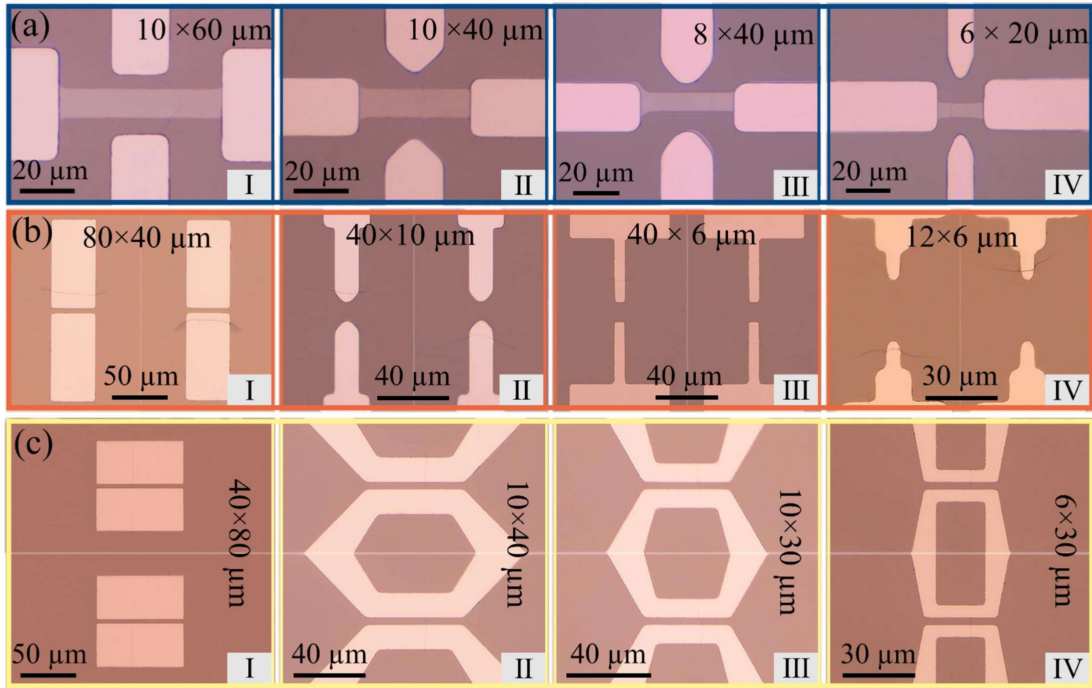

Figure E2 Precise control of crack formation and switching with different device configurations. (a) Switching of single-crack-based device; (b) Complementary switching of two-crack-based device; (c) Complementary switching of single-crack-based device.

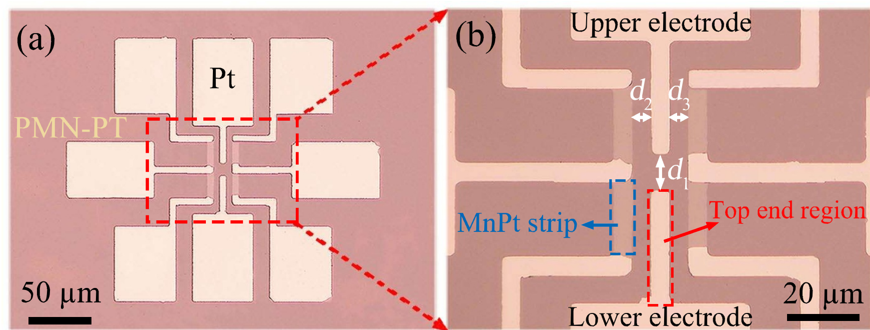

Figure F1 (a) The full-size optical images of the two-crack based device with separate input and output signal paths; (b) The enlarged detail view of the central region.

2 Luo Q, Guo Z, Huang H B, et al. Nanoelectromechanical switches by controlled switchable cracking. IEEE Electron Device Lett, 2019, 29: 131C133

3 Liu Z Q, Biegalski M D, Hsu S-L, et al. Epitaxial growth of intermetallic MnPt films on oxides and large exchange bias. Adv Mater, 2016, 27: 118C123

4 Sun E W, Cao W W. Relaxor-based ferroelectric single crystals: growth, domain engineering, characterization and applications. Prog Mater Sci, 2014, 65: 124-210

5 Peng J, Luo H S, He T H, et al. Elastic, dielectric, and piezoelectric characterization of 0.70Pb(Mg1/3Nb2/3)O3-0.30PbTiO3 single crystals. Mater Lett, 2005, 59: 640-643

6 Luo Q, Guo Z, Zhang S, et al. Crack-based complementary nanoelectromechanical switches for reconfigurable computing. IEEE Electron Device Lett, 2020, 41: 784C787

7 Guo Z, Luo Q, Huang H B, et al. Low-energy complementary ferroelectric-nanocrack logic. Nano Energy, 2020, 75: 104871

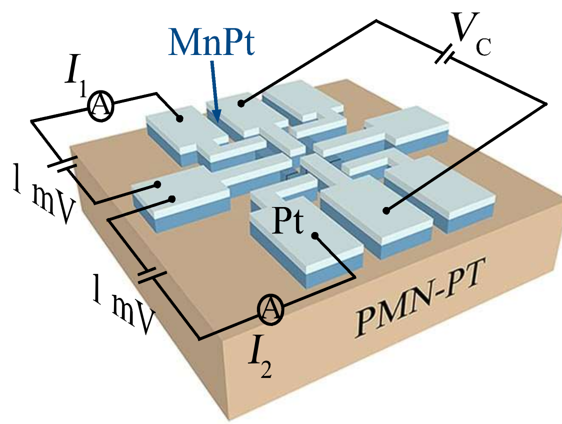

Figure F2 Schematic of the device structure and resistance measurement setup.